Optimising the efficiency of pulsed diode pumped Yb:YAG laser amplifiers for ns pulse generation.

K. Ertel,[1,*] S. Banerjee,[1] P. D. Mason,[1] P. J. Phillips,[1] M. Siebold,[2] C. Hernandez-Gomez,[1] and J. C. Collier[1]

[1]*Central Laser Facility, STFC Rutherford Appleton Laboratory, Didcot, OX11 0QX, UK*

[2]*Helmholtz Center Dresden-Rossendorf, Bautzner Landstr. 400, 01328 Dresden, Germany*

**klaus.ertel@stfc.ac.uk*

Abstract: We present a numerical model of a pulsed, diode-pumped Yb:YAG laser amplifier for the generation of high energy ns-pulses. This model is used to explore how optical-to-optical efficiency depends on factors such as pump duration, pump spectrum, pump intensity, doping concentration, and operating temperature. We put special emphasis on finding ways to achieve high efficiency within the practical limitations imposed by real-world laser systems, such as limited pump brightness and limited damage fluence. We show that a particularly advantageous way of improving efficiency within those constraints is operation at cryogenic temperature. Based on the numerical findings we present a concept for a scalable amplifier based on an end-pumped, cryogenic, gas-cooled multi-slab architecture.

OCIS codes: (140.3280) Laser amplifiers; (140.3538) Lasers, pulsed; (140.3615) Lasers, ytterbium; (140.5560) Pumping.

References and links

1. A. C. Erlandson, S. M. Aceves, A. J. Bayramian, A. L. Bullington, R. J. Beach, C. D. Boley, J. A. Caird, R. J. Deri, A. M. Dunne, D. L. Flowers, M. A. Henesian, K. R. Manes, E. I. Moses, S. I. Rana, K. I. Schaffers, M. L. Spaeth, C. J. Stolz, and S. J. Telford, "Comparison of Nd:phosphate glass, Yb:YAG and Yb:S-FAP laser beamlines for laser inertial fusion energy (LIFE) [Invited]," Opt. Mater. Express **1,** 1341–1352 (2011) `http://www.opticsinfobase.org/ome/abstract.cfm?URI=ome-1-7-1341`
2. J. Faure, Y. Glinec, A. Pukhov, S. Kiselev, S. Gordienko, E. Lefebvre, J. Rousseau, F. Burgy, and V. Malka, "A laser-plasma accelerator producing monoenergetic electron beams," Nature **431,** 541–544 (2004).
3. H. Schwoerer, S. Pfotenhauer, O. Jackel, K. Amthor, B. Liesfeld, W. Ziegler, R. Sauerbrey, K. Ledingham, and T. Esirkepov, "Laser-plasma acceleration of quasi-monoenergetic protons from microstructured targets," Nature **439,** 445–448 (2006).
4. S. Kneip, S. R. Nagel, C. Bellei, N. Bourgeois, A. E. Dangor, A. Gopal, R. Heathcote, S. P. D. Mangles, J. R. Marquès, A. Maksimchuk, P. M. Nilson, K. T. Phuoc, S. Reed, M. Tzoufras, F. S. Tsung, L. Willingale, W. B. Mori, A. Rousse, K. Krushelnick, and Z. Najmudin, "Observation of synchrotron radiation from electrons accelerated in a petawatt-laser-generated plasma cavity," Phys. Rev. Lett. **100,** 105006 (2008).
5. V. Malka, J. Faure, Y. A. Gauduel, E. Lefebvre, A. Rousse, and K. T. Phuoc, "Principles and applications of compact laser-plasma accelerators," Nat. Phys. **4,** 447–453 (2008).
6. E. Esarey, C. B. Schroeder, and W. P. Leemans, "Physics of laser-driven plasma-based electron accelerators," Rev. Mod. Phys. **81,** 1229–1285 (2009).
7. M. Dunne, "A high-power laser fusion facility for Europe," Nat. Phys. **2,** 2–5 (2006).
8. "The HiPER project," `http://www.hiper-laser.org`.
9. J.-P. Chambaret, O. Chekhlov, G. Cheriaux, J. Collier, R. Dabu, P. Dombi, A. M. Dunne, K. Ertel, P. Georges, J. Hebling, J. Hein, C. Hernandez-Gomez, C. Hooker, S. Karsch, G. Korn, F. Krausz, C. L. Blanc, Z. Major, F.

#157898 - $15.00 USD Received 11 Nov 2011; revised 5 Dec 2011; accepted 5 Dec 2011; published 14 Dec 2011

Mathieu, T. Metzger, G. Mourou, P. Nickles, K. Osvay, B. Rus, W. Sandner, G. Szabó, D. Ursescu, and K. Varjú, "Extreme Light Infrastructure: laser architecture and major challenges," Proc. SPIE **7721,** 77211D (2010).
10. "ELI - the Extreme Light Infrastructure, " http://www.extreme-light-infrastructure.eu.
11. G. Miller, E. Moses, and C. Wuest, "The national ignition facility," Opt. Eng. **43,** 2841–2853 (2004).
12. M. Andre, "The French megajoule laser project (LMJ)," Fusion Eng. Des. **44,** 43–49 (1999).
13. C. Danson, P. Brummitt, R. Clarke, J. Collier, B. Fell, A. Frackiewicz, S. Hancock, S. Hawkes, C. Hernandez-Gomez, P. Holligan, M. Hutchinson, A. Kidd, W. Lester, I. Musgrave, D. Neely, D. Neville, P. Norreys, D. Pepler, C. Reason, W. Shaikh, T. Winstone, R. Wyatt, and B. Wyborn, "Vulcan Petawatt - an ultra-high-intensity interaction facility," Nucl. Fusion **44,** 239–246 (2004).
14. R. M. Yamamoto, J. M. Parker, K. L. Allen, R. W. Allmon, K. F. Alviso, C. P. J. Barty, B. S. Bhachu, C. D. Boley, A. K. Burnham, R. L. Combs, K. P. Cutter, S. N. Fochs, S. A. Gonzales, R. L. Hurd, K. N. LaFortune, W. J. Manning, M. A. McClelland, R. D. Merrill, L. Molina, C. W. Parks, P. H. Pax, A. S. Posey, M. D. Rotter, B. M. Roy, A. M. Rubenchik, T. F. Soules, and D. E. Webb, "Evolution of a solid state laser," Proc. SPIE **6552,** 655205 (2007).
15. A. Bayramian, P. Armstrong, E. Ault, R. Beach, C. Bibeau, J. Caird, R. Campbell, B. Chai, J. Dawson, C. Ebbers, A. Erlandson, Y. Fei, B. Freitas, R. Kent, Z. Liao, T. Ladran, J. Menapace, B. Molander, S. Payne, N. Peterson, M. Randles, K. Schaffers, S. Sutton, J. Tassano, S. Telford, and E. Utterback, "The Mercury project: a high average power, gas-cooled laser for inertial fusion energy development," Fusion Sci. Technol. **52,** 383–387 (2007).
16. D. Albach, M. Arzakantsyan, G. Bourdet, J.-C. Chanteloup, P. Hollander, and B. Vincent, "Current status of the LUCIA laser system," J. Phys.: Conf. Ser. **244,** 032015 (2010).
17. J. Hein, S. Podleska, M. Siebold, M. Hellwing, R. Bodefeld, R. Sauerbrey, D. Ehrt, and W. Wintzer, "Diode-pumped chirped pulse amplification to the joule level," Appl. Phys. B **79,** 419–422 (2004).
18. T. Fan, "Optimizing the efficiency and stored energy in quasi-three-level lasers," IEEE J. Quantum Electron. **28,** 2692 –2697 (1992).
19. G. Bourdet and O. Casagrande, "Effect of diode wavelength broadening in a diode end-pumped solid-state amplifier," Appl. Opt. **46,** 2709–2716 (2007).
20. M. Siebold, M. Loeser, U. Schramm, J. Koerner, M. Wolf, M. Hellwing, J. Hein, and K. Ertel, "High-efficiency, room-temperature nanosecond Yb:YAG laser," Opt. Express **17,** 19887–19893 (2009), http://www.opticsinfobase.org/abstract.cfm?URI=oe-17-22-19887.
21. P. Lacovara, H. K. Choi, C. A. Wang, R. L. Aggarwal, and T. Y. Fan, "Room-temperature diode-pumped Yb:YAG laser," Opt. Lett. **14,** 1089–1091 (1991).
22. T. Kasamatsu, H. Sekita, and Y. Kuwano, "Temperature dependence and optimization of 970-nm diode-pumped Yb:YAG and Yb:LuAG lasers," Appl. Opt. **38,** 5149–5153 (1999).
23. D. C. Brown, R. L. Cone, Y. C. Sun, and R. W. Equall, "Yb:YAG absorption at ambient and LF cryogenic temperatures," IEEE J. Sel. Top. Quantum Electron. **11,** 604–612 (2005).
24. A. Siegman, *Lasers*, (University Science Books, 1986).
25. J. B. Trenholme, "Fluorescence amplification and parasitic oscillation limitations in disc lasers," Naval Research Laboratory Memorandum Rep. 2480, 1972.
26. D. Albach, J.-C. Chanteloup, and G. Le Touzé, "Influence of ASE on the gain distribution in large size, high gain Yb^{3+}:YAG slabs," Opt. Express **17,** 3792–3801 (2009), http://www.opticsexpress.org/abstract.cfm?URI=oe-17-5-3792.
27. G. Bogomolova, D. Vylegzhanin, and A. Kaminskii, "Spectral and lasing investigations of garnets with Yb^{3+} ions," Sov. Phys. JETP **42,** 440–446 (1975).
28. D. J. Richardson, J. Nilsson, and W. A. Clarkson, "High power fiber lasers: current status and future perspectives," J. Opt. Soc. Am. B **27,** 63–92 (2010).
29. A. Giesen and J. Speiser, "Fifteen years of work on thin-disk lasers: results and scaling laws," IEEE J. Sel. Top. Quantum Electron. **13,** 598–609 (2007).
30. S. Nakai and K. Mima, "Laser driven inertial fusion energy: present and prospective," Rep. Prog. Phys. **67,** 321-349 (2004).
31. K. Ertel, C. Hooker, S. J. Hawkes, B. T. Parry, and J. L. Collier, "ASE suppression in a high energy titanium sapphire amplifier," Opt. Express **16**, 8039–8049 (2008), http://www.opticsinfobase.org/oe/abstract.cfm?URI=oe-16-11-8039.
32. H. Yagi, J. F. Bisson, K. Ueda, and T. Yanagitani, "$Y_3Al_5O_{12}$ ceramic absorbers for the suppression of parasitic oscillation in high-power Nd:YAG lasers," J. Lumin. **121,** 88–94 (2006).
33. S. B. Sutton and G. F. Albrecht, "Thermal management in inertial fusion energy slab amplifiers," Proc. SPIE **2633**, 272–281 (1995).
34. R. L. Aggarwal, D. J. Ripin, J. R. Ochoa, and T. Y. Fan, "Measurement of thermo-optic properties of $Y_3Al_5O_{12}$, $Lu_3Al_5O_{12}$, $YAlO_3$, $LiYF_4$, $LiLuF_4$, BaY_2F_8, $KGd(WO_4)_2$, and $KY(WO_4)_2$ laser crystals in the 80-300 K temperature range," J. Appl. Phys. **98,** 103514 (2005).
35. T. Y. Fan, D. J. Ripin, R. L. Aggarwal, J. R. Ochoa, B. Chann, M. Tilleman, and J. Spitzberg, "Cryogenic Yb^{3+}-doped solid-state lasers," IEEE J. Sel. Top. Quantum Electron. **13,** 448–459 (2007).
36. J. Dong, M. Bass, Y. Mao, P. Deng, and F. Gan, "Dependence of the Yb^{3+} emission cross section and lifetime on

#157898 - $15.00 USD Received 11 Nov 2011; revised 5 Dec 2011; accepted 5 Dec 2011; published 14 Dec 2011

temperature and concentration in yttrium aluminum garnet," J. Opt. Soc. Am. B **20**, 1975–1979 (2003).
37. J. Körner, J. Hein, M. Kahle, H. Liebetrau, M. Lenski, M. Kaluza, M. Loeser, and M. Siebold, "Temperature dependent measurement of absorption and emission cross sections for various Yb^{3+} doped laser materials," Proc. SPIE **8080,** 808003 (2011).
38. K. Ertel, S. Banerjee, C. Hernandez-Gomez, P. D. Mason, J. Phillips, and J. Collier, "Performance Modelling of a 1 kJ DPSSL System," in *High Intensity Lasers and High Field Phenomena,* OSA Technical Digest (CD) (Optical Society of America, 2011), paper HThE3.
39. P. D. Mason, K. Ertel, S. Banerjee, P. J. Phillips, C. Hernandez-Gomez, and J. L. Collier, "Optimised design for a 1 kJ diode-pumped solid-state laser system," Proc. SPIE **8080,** 80801X (2011).

1. Introduction

Harnessing the potential of high-intensity laser-matter interactions and developing them into practical industrial, medical, and scientific applications will require lasers producing ns-pulses at multi-Hz (typically 10 Hz) repetition rate, with energies up to the kJ-level, at an overall electrical-to-optical efficiency exceeding 10 %, and with a lifetime of several billion shots. The generated ns pulses can be used directly for generating dense plasmas, for example for energy production through inertial confinement fusion [1], or to pump amplifiers for fs-pulse generation such as OPCPA or Ti:Sapphire chains. The generated fs-pulses, with up to multi-PW peak powers, can then be used to drive secondary sources producing ultra-short and ultra-brilliant bursts of either electromagnetic radiation (ranging from THz to hard X-rays), or of particles such as electrons, neutrons, protons or heavier ions [2–6]. Prominent projects dedicated to the development of such real world applications include HiPER and ELI [7–10].

Currently used flashlamp-pumped Nd:Glass laser systems [11–13] are not able to fulfil these requirements as their repetition rate, efficiency, and lifetime all fall short by several orders of magnitude. Diode pumped solid state lasers (DPSSLs) offer an alternative that can achieve these goals. One of the most promising gain media for such high energy, high repetition rate DPSSL systems is Yb^{3+}doped YAG (Yb:YAG). Yb^{3+} as an active laser ion offers very long fluorescence lifetimes, a low quantum defect, reasonable gain cross sections, and efficient and reliable high power laser diodes are readily available at its pump wavelength. The simple energy level structure of Yb^{3+} also avoids detrimental effects such as excited state absorption, upconversion and concentration quenching. YAG as the host medium offers good thermo-mechanical and thermo-optical properties, and, if it is used in its ceramic form, it can be produced in very large sizes [14] with good optical quality. The last point is especially important for kJ-class laser systems as they will require amplifier stages with apertures in excess of 10 cm.

Existing high energy DPSSL projects based on Yb-doped media include Mercury [15], LUCIA [16], and Polaris [17]. The first numerical calculations of the efficiency of a pulsed, energy-storage Yb:YAG laser were presented by Fan [18], who introduced the concept of an optimum absorption length and also explored the effects of multi-pass pumping. The effects of a non-monochromatic pump spectrum were first explored by Bourdet and Casagrande [19], by introducing an effective absorption cross section. However, this did not take into account the changing shape of the pump beam spectrum as it propagates through the laser medium. It was also incorrectly stated that a broadened pump spectrum will incur no loss in efficiency, as long as the reduced absorption is compensated by an increased gain medium length. The efficiency gain that can be realised by cooling the laser medium to cryogenic temperatures was first explored by Siebold et al [20]. We will expand on those considerations in this paper and present a comprehensive model that explores the complex interplay between numerous factors affecting optical-to-optical efficiency. We will specifically explore how the influence of factors such as gain medium doping and thickness, pump fluence, and pump spectrum differs for room and cryogenic temperature operation.

Based on the experience of the aforementioned projects and on the results of our numerical

#157898 - $15.00 USD Received 11 Nov 2011; revised 5 Dec 2011; accepted 5 Dec 2011; published 14 Dec 2011

modelling we have devised a new scalable and efficient architecture for an end-pumped, cryogenically cooled Yb:YAG amplifier. In the following sections we present a model for predicting laser-physical parameters of such an amplifier, which then allows optimisation of optical-to-optical efficiency, within the practical constraints imposed by available diode technology, damage threshold of optical materials, and amplified spontaneous emission (ASE) losses. A conceptual design for a large aperture amplifier is described in Section 4.

2. Amplifier efficiency

2.1. Loss mechanisms

The quantity of interest is the overall optical-to-optical efficiency which is the product of the pump efficiency η_P and the extraction efficiency η_{ex}, with η_P defined as E_{acc}/E_P, where E_P is the pump energy and E_{acc} the part of the stored energy that is accessible for extraction. Not all the stored energy is accessible due to the quasi-3-level nature of the laser medium. The definition of η_{ex} is E_{out}/E_{acc}, where E_{out} is the energy of the amplified laser pulse at the output of the system. Because we are discussing the amplification of pulses whose duration (nanoseconds) is much shorter than the fluorescence lifetime (1 ms), pumping and extraction can be treated separately. In the following we shall mainly concentrate on η_P, which is determined by the sum of the pumping-related losses or by the product of the efficiencies η_i associated with those losses. The corresponding loss mechanisms are:

1. The quantum defect, with associated efficiency η_{QD}.
2. The fluorescence decay, with associated efficiency η_{fl}.
3. Amplified spontaneous emission (ASE).
4. Incomplete absorption of the pump light, with associated efficiency η_{abs}.
5. The in-accessible upper state population that is required to compensate for the population in the lower laser level (due to the quasi-3-level nature of the Yb-doped material) in order to overcome reabsorption, with associated efficiency η_{reabs}.

A brief overview of each loss mechanism is given in the following sections.

2.1.1. Quantum defect

The quantum defect is a consequence of the energy difference between lasing photons and pump photons. The associated efficiency is given by $\eta_{QD} = \lambda_P/\lambda_L$, where λ_P and λ_L are the pump and lasing wavelengths, respectively. One advantage of Yb-doped materials is their small quantum defect, the downside of which is their quasi-3-level nature. To maximise η_{QD}, the difference between λ_P and λ_L should be minimised. In strongly pumped Yb:YAG systems, which are considered here, $\lambda_L = 1030\,\text{nm}$ [21]. The closest possible λ_P is 969 nm, the so-called zero-phonon line. However, the narrow width of this line makes it impracticable for diode pumping [22, 23] and therefore a λ_P near 940 nm is usually chosen, with a corresponding $\eta_{QD} = 91\,\%$.

2.1.2. Fluorescence loss

An amplifier for laser pulses needs to be pumped for a finite time in order to accumulate energy in the form of excited ions. During the pumping process, some of these atoms will decay spontaneously by emitting a fluorescence photon. The formula for η_{fl} [24] reads

$$\eta_{fl} = \frac{\tau_{fl}}{T_P}\left(1 - \exp\left(-\frac{T_P}{\tau_{fl}}\right)\right), \tag{1}$$

#157898 - $15.00 USD Received 11 Nov 2011; revised 5 Dec 2011; accepted 5 Dec 2011; published 14 Dec 2011

where τ_{fl} is the fluorescence lifetime and T_P is the duration of the pump pulse (assuming constant pump power). The amount of stored energy E_{st} on the other hand reads

$$E_{st} = R_P \tau_{fl} \left(1 - \exp\left(-\frac{T_P}{\tau_{fl}}\right)\right). \tag{2}$$

For a given pumping rate R_P, which is proportional to the pump intensity, the storable energy is therefore directly proportional to τ_{fl}. Equation (2) indicates that E_{st} grows with T_P whereas Eq. (1) indicates that η_{fl} decreases with T_P, a fact illustrated in Fig. 1. In principle, fluorescence losses could be almost completely eliminated through use of very short pump pulses with $T_P \ll \tau_{fl}$. Practically, it then becomes difficult to deliver enough energy because of the limited brightness and the high cost per unit peak power of pump laser diodes. Hence, choosing $T_P = \tau_{fl}$ for which $\eta_{fl} = 63\%$ and E_{st} is 63% of the maximum possible value offers a good compromise between efficiency and required number of diodes.

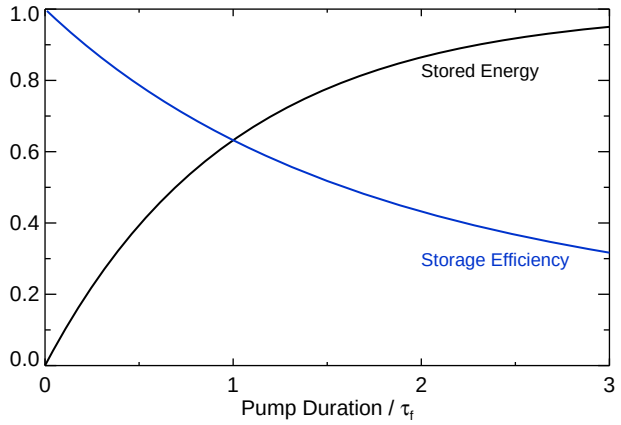

Fig. 1. Impact of fluorescence loss on stored energy and storage efficiency.

2.1.3. Amplified spontaneous emission

ASE is another loss mechanism reducing the achievable η_P. Photons emitted by spontaneous fluorescence travelling through the pumped gain medium can de-excite other ions by way of stimulated emission, therefore leading to additional losses and effectively reducing τ_{fl}. In the extreme case, if optical feedback caused by Fresnel reflections from the surfaces of the gain medium is strong enough ASE can develop into undesirable parasitic lasing. We shall not provide a quantitative treatment of ASE in this article but would like to refer to other in-depth quantitative model calculations both from the early days of high energy laser amplifiers [25], and from the recent past [26]. There are two design rules that can be deduced from such calculations. Firstly, the maximum gain-length product found in an amplifier should not exceed a certain value. Secondly the optical feedback caused by Fresnel reflections from surfaces needs to be suppressed as strongly as possible. These rules have been incorporated in the conceptual design presented in Section 4.

2.1.4. Reabsorption and pump absorption

In a pure 4-level system reabsorption is absent ($\eta_{reabs} = 1$) and pump absorption can be maximised by increasing doping level and thickness of the gain material. In a quasi-3-level system, pump absorption and reabsorption need to be balanced against each other since too high doping

#157898 - $15.00 USD Received 11 Nov 2011; revised 5 Dec 2011; accepted 5 Dec 2011; published 14 Dec 2011

levels would lead to excessive reabsorption losses. The factors that influence the product of the two efficiencies $\eta_{abs}\eta_{reabs}$, and hence the overall pump efficiency, shall be discussed in detail in the following sections. As there is no straightforward analytical expression for $\eta_{abs}\eta_{reabs}$ that takes into account effects like saturated absorption and wavelength dependent absorption cross sections, we have used a numerical model to assess the impact of various parameters on η_P. This was also used to evaluate how η_P can be optimised within the constraints posed by real-world optical components, for instance laser diodes with limited brightness and finite spectral width, and optical components with limited laser damage threshold.

2.1.5. Extraction efficiency

The limits imposed on extraction efficiency are mostly of a practical rather than fundamental nature. In the following we give a non-exhaustive list of factors affecting extraction efficiency and how these factors can be optimised to maximise efficiency.

- **Overlap between pump and extraction beams:** to achieve maximum overlap, both beams should show a uniform, ideally top-hat shaped intensity distribution, low divergence and collinear propagation. Because of the finite brightness of high-power laser diodes, pump beam divergence grows with intensity, therefore favouring amplifier schemes with low pump fluence.

- **Optical losses:** the influence of losses can be reduced by minimising the total number of optical elements in the beam path. This means that amplifier architectures with high single-pass gain are favourable as they enable effective energy extraction in a low number of passes. However, this needs to be balanced against the increased risk of ASE.

- **Laser damage and nonlinear effects:** these effects can be minimised by reducing the the fluence of the extraction pulses and also the overall path travelled inside optical materials. An amplifier with a low saturation fluence enables effective energy extraction at low fluence and over a small number of passes. Low saturation fluence also equates to high gain cross sections, meaning that high small-signal gain can be achieved at low pump fluence, which also helps to mitigate the effects mentioned previously.

In Section 4 we shall describe the conceptual design of a large-aperture amplifier that strikes a compromise between the partly conflicting requirements for high pump and extraction efficiency. With this concept, we can achieve high pump efficiency and high small-signal gain at moderate pump and extraction fluences.

2.2. Description of model

In our model we simulate optical pumping of a Yb:YAG laser amplifier that is end pumped (also called face pumped) by a pump pulse of duration T_P and constant intensity I_P. The pump light propagates along the z-axis which is also the optical axis. The doping concentration is N, which can vary along the optical axis, in which case it becomes $N(z)$. The model can handle single and double sided pumping, transmission and active mirror type geometries, as well as multi-pass pumping.

Figure 2 shows an illustration of the energy level scheme of Yb^{3+}, it consists of a lower (LM) and an upper manifold (UM), each containing a number of Stark levels [27]. Optical pumping excites ions from the ground state (GS) to the pump level (PL) from where they relax into the upper laser level (UL). Spontaneous or stimulated emission de-excites these ions to the lower laser level (LL) from which they relax back to GS. Because of the small energy separation between GS and LL, LL exhibits a significant thermal population at room temperature which is

#157898 - $15.00 USD Received 11 Nov 2011; revised 5 Dec 2011; accepted 5 Dec 2011; published 14 Dec 2011

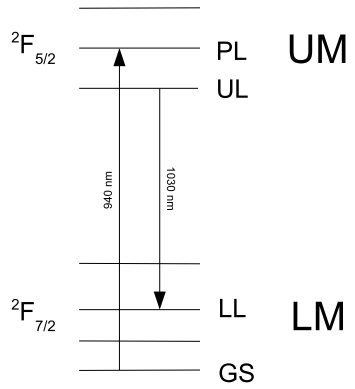

Fig. 2. Level scheme of Yb:YAG. UM, LM: upper and lower manifold; GS: ground state; LL and UL: lower and upper laser level; PL: pump level.

determined by the Boltzmann factor

$$f_{LL} = \exp(-E_{LL}/kT) \,/ \sum_i \exp(-E_i/kT), \tag{3}$$

where f_i stands for the fraction of atoms residing in level i, and E_i stands for the energy of level i. For Yb:YAG, $E_{LL} = 612\,\mathrm{cm}^{-1}$ and $f_{LL} = 4.6\%$ at 300 K. The fraction of excited atoms, i.e. the fraction residing in UM is called β which is zero at the start of the pump pulse. We assume that thermal equilibrium between the sub-levels in LM is maintained at all times, hence the population density in LL reads $N_{LL} = (1-\beta) f_{LL} N$. In order to overcome reabsorption and to achieve gain at the lasing wavelength, a minimum excited fraction $\beta_{min} = f_{LL}/(1+f_{LL})$ needs to be established, so that $N_{UL} = N_{LL}$, where N_{UL} is the population density in UL. In a low repetition rate ($f_{rep} \ll \tau_{fl}^{-1}$) amplifier β_{min} needs to be re-established from zero for every shot. Reabsorption therefore plays a more important role than in cw or high repetition rate systems. We neglect the thermal distribution in UM and assume that all excited ions reside in UL.

During pumping, ions are excited from the ground state to the pump level at a rate

$$\frac{\partial N_U}{\partial t} = (1-\beta) N \frac{I_P \sigma_{abs}}{h\nu_P}, \tag{4}$$

where $N_U = N\beta$ is the population density in the upper manifold, σ_{abs} the pump absorption cross section, and ν_P the pump light frequency. In our computer model, this rate equation is solved numerically, taking into account pump depletion as the pump propagates through the gain medium, saturation of the pump absorption, fluorescence decay (assuming $\tau_f = 1\,\mathrm{ms}$), the wavelength-dependence of σ_{abs} and I_P, and a doping concentration N that can vary along the optical axis. Quantities of interest are β at the end of the pump pulse, and the unabsorbed fraction of the pump energy. Quantities that can then be derived are the small-signal gain coefficient $g_o = \sigma_e(N_{UL} - N_{LL}) = \sigma_e N(\beta - f_{LL}(1-\beta))$ and the accessible energy density $\tilde{E}_{acc} = Nh\nu_L(\beta - \beta_{min})$ where σ_e is the stimulated emission cross section and ν_L is the lasing frequency . Integrating g_o and $\tilde{E}_{acc}$ along the optical axis yields the small-signal gain and accessible fluence, respectively.

3. Modelling and optimisation of pump efficiency

In the following we shall present results obtained with our computer model in order to illustrate how η_P depends on various factors and how it can be optimised. Special emphasis is put on

#157898 - $15.00 USD Received 11 Nov 2011; revised 5 Dec 2011; accepted 5 Dec 2011; published 14 Dec 2011

the pump and extraction fluence levels that are required to achieve good efficiency. It is already clear from basic principles that very high fluence levels are required at room temperature. The reason for this is that to achieve good efficiency, a very strong inversion with $\beta \gg \beta_{min}$ needs to be established. As $\beta_{min} = 4.4\,\%$, β needs to be of order 50 %, which in turn means that pump fluences higher than the pump saturation fluence $\frac{h\nu}{\sigma_{abs}} \approx 25\,\mathrm{J\,cm^{-2}}$ are needed. Reducing f_{LL} and hence β_{min} by cooling the laser medium therefore offers a straightforward way of reaching high efficiencies at manageable fluence levels. Cooling the active medium to 164 K reduces f_{LL} by a factor of 10 and cooling to 114 K by a factor of 100.

3.1. Modelled scenarios

We use two baseline scenarios to explore the behaviour of η_P. Both are based on an amplifier longitudinally pumped from both sides. The scenarios are chosen to illustrate the differences when operating at gain medium temperatures of 300 K (room temperature) and of 175 K. The baseline parameters were chosen such that they are roughly commensurate with an output fluence (fluence of the amplified beam) of $5\,\mathrm{J\,cm^{-2}}$, which is deemed the maximum level at which optical damage can safely be avoided in long-term operation (for the few-ns pulse durations under consideration). The parameters for pump intensity and pump spectral width were also chosen such that they are achievable with standard high power laser diode stacks. The baseline parameters are listed in Table 1. In the following sections, the effects of varying one parameter while keeping the others constant are explored.

Table 1. Model parameters for baseline scenarios. I_P: combined pump intensity, N_{col}: columnar doping density (see Section 3.3), T_P: pump duration, $\Delta\lambda_P$: FWHM-width of Gaussian-shaped pump spectrum, $\lambda_{c,P}$: centre wavelength of pump spectrum. Optimum means that for a given set of other parameters, the particular parameter is chosen such that η_P is maximised.

Scenario	Temperature	I_P	T_P	N_{col}	$\Delta\lambda_P$	$\lambda_{c,P}$
Room temperature	300 K	$20\,\mathrm{kW\,cm^{-2}}$	1 ms	optimum	5 nm	optimum
Low temperature	175 K	$10\,\mathrm{kW\,cm^{-2}}$	1 ms	optimum	5 nm	optimum

3.2. Effect of quantum defect and pump duration

The effect of these two parameters can be treated analytically, as explained in Section 2.1. In our scenarios they limit the maximum achievable η_P to 57.7 %. This is already significantly below the maximum efficiencies that have been demonstrated for cw Yb-doped lasers [28, 29]. Applications which are very sensitive to efficiency like laser fusion energy production may therefore require shorter pump durations, even if that results in significantly higher costs for the pump laser diodes [1, 30].

3.3. Effect of doping and thickness

The first observation when varying doping concentration N and thickness L of the amplifier was that η_P is constant for a constant product $N \times L$. Therefore the so-called area or columnar doping density $N_{col} = N \times L$ is introduced which is then the only relevant parameter in the context of optimising η_P. It was also found that η_P is not affected by non-constant doping concentrations (along the optical axis), again as long as N_{col} is held constant. The expression for N_{col} then reads $N_{col} = \int_0^L N(z)\mathrm{d}z$. In fact, η_P only depends on the average β in the gain medium, which is not affected by the doping distribution, nor by the pumping geometry, as long as longitudinal single-pass pumping is used, as shall be shown in the following paragraph. The possibility to

#157898 - $15.00 USD Received 11 Nov 2011; revised 5 Dec 2011; accepted 5 Dec 2011; published 14 Dec 2011

vary N and L and to introduce non-constant doping profiles is of great importance and helps to overcome conflicting constraints when designing an amplifier, as shall be explored in Section 4.

The effect of varying N_{col} is illustrated in Fig. 3, where the doping concentration N is expressed in atomic %, with 1% equating to $N = 1.39 \times 10^{20}\,\mathrm{cm}^{-3}$. It can be seen that there is indeed a maximum where the effect of low pump absorption, which dominates at small N_{col}, is balanced against the effect of reabsorption, which dominates at high N_{col}. As the effect of reabsorption is greatly reduced at 175 K, the optimum N_{col} is significantly higher, contributing to an improved efficiency through increased pump absorption (along with the reduced reabsorption). At optimum N_{col}, 89.2% and 97.1% of the pump light is absorbed in the room temperature and low temperature scenarios, respectively. Curves for slightly higher and lower pump intensities are also plotted in Fig. 3. These illustrate that η_P rises with growing I_P, as does the optimum N_{col}. For a given I_P, η_P is significantly higher in the low temperature case and is achieved at a higher N_{col}. At low temperature, η_P is also less sensitive to variations in N_{col}.

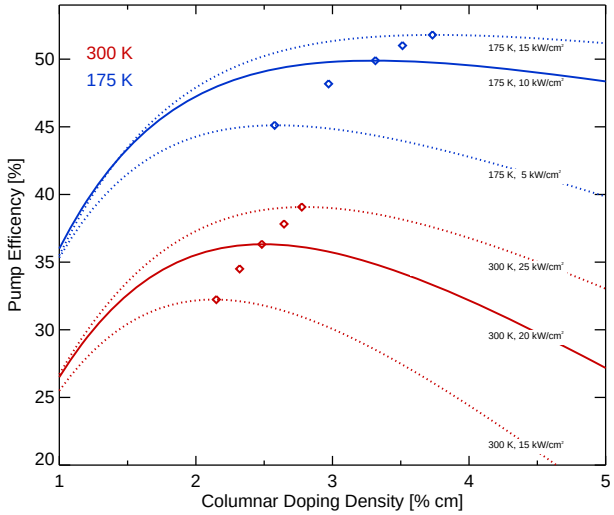

Fig. 3. Pump efficiency as function of columnar doping density. Shown are the results for the two scenarios (solid lines) and for pump intensities differing by $\pm 5\,\mathrm{kW\,cm}^{-2}$ from the scenario values (dotted lines). Also shown is the location of the optimum operating points for different pump intensities (diamonds) within this range.

The spatially resolved upper state population $\beta(z)$ for optimum N_{col} (assuming a constant doping level) is shown in Fig. 4. It is noteworthy that β stays well above β_{min}. This is in contrast to an amplifier with single-sided pumping where the optimum N_{col} is reached if $\beta = \beta_{min}$ at the point with the lowest β. Hence $\beta(z)$ shows a less uniform distribution in single-sided pumped amplifiers. This is undesirable for various reasons, in particular for ASE management where higher inversion values, and hence gain coefficients, will lead to increased losses and to a higher risk of parasitic oscillations. Maximum η_P and optimum N_{col}, however, do not differ for single and double-sided pumping as the average β remains the same.

3.4. Effect of pump intensity

The effect of pump intensity on η_P is shown in Fig. 5. For each data point the optimum N_{col} was chosen. Several facts can be inferred from the graph. Firstly, η_P grows with pump intensity. Secondly, η_P is generally higher at low temperature, especially for lower pump intensities. Thirdly, a minimum pump intensity is required to achieve any gain at all in the amplifier. At

#157898 - $15.00 USD Received 11 Nov 2011; revised 5 Dec 2011; accepted 5 Dec 2011; published 14 Dec 2011

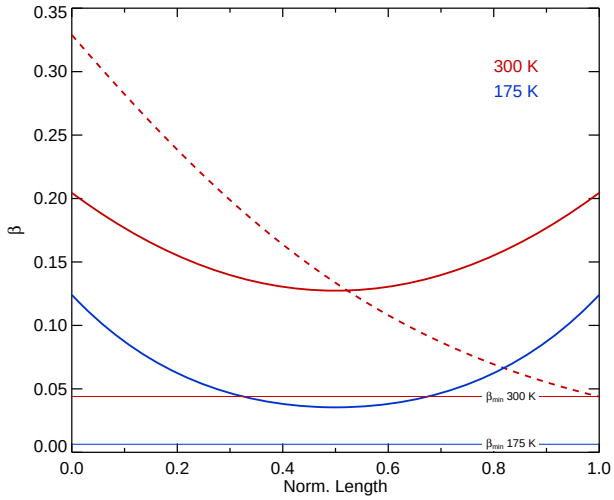

Fig. 4. Distribution of upper state population β along amplifier optical axis. Shown are results for room temperature (red) and low temperature (blue) scenarios. Also shown are results for room temperature scenario with single-sided pumping (dashed line) and values for β_{min} (horizontal lines) at room temperature and at 175 K.

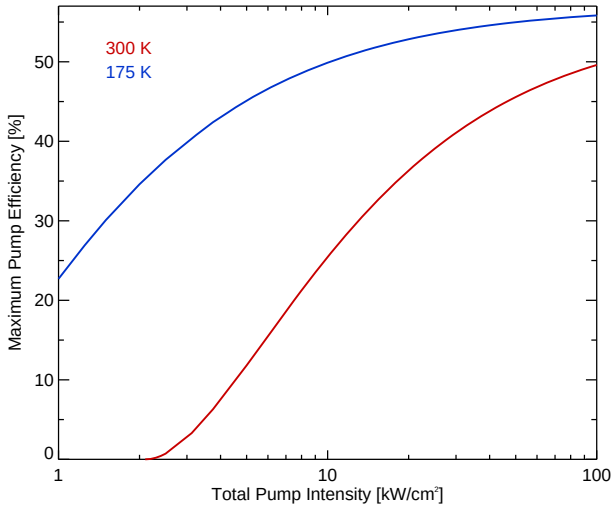

Fig. 5. Maximum pump efficiency as function of pump intensity for room temperature scenario (red) and low temperature scenario (blue).

300 K, this minimum is 2.1 kW cm^{-2}, whereas at 175 K the minimum is only 0.25 kW cm^{-2} (not visible in Fig. 5 due to the chosen logarithmic scale). Below this minimum intensity $\beta < \beta_{min}$ and the amplifier is absorbing. In practice, it will be difficult to achieve pump intensities much beyond 10 kW cm^{-2} and also to manage the high extraction fluence levels that go with such high pump fluences. Together with other advantages, which will be described in the following sections, low temperature operation is therefore a highly attractive option for high energy Yb:YAG amplifiers. We shall present the concept of such an amplifier in Section 4.

#157898 - $15.00 USD Received 11 Nov 2011; revised 5 Dec 2011; accepted 5 Dec 2011; published 14 Dec 2011

3.5. *Effect of pump spectrum*

So far, all results have been derived assuming a Gaussian-shaped pump spectrum with a 5 nm width (FWHM), centred at a wavelength near 940 nm that yields the highest η_P. The spectral change (chirp) that occurs during the pump pulse due to internal heating of the laser diodes is not taken into account here. This could, however, easily be integrated into the model as it does treat the pumping process in a time-resolved fashion. The spectrally resolved absorption cross sections at 300 K and 175 K were taken from [23]. The two absorption spectra are shown in Fig. 6, together with a 5 nm FWHM pump spectrum centred at 939 nm for comparison.

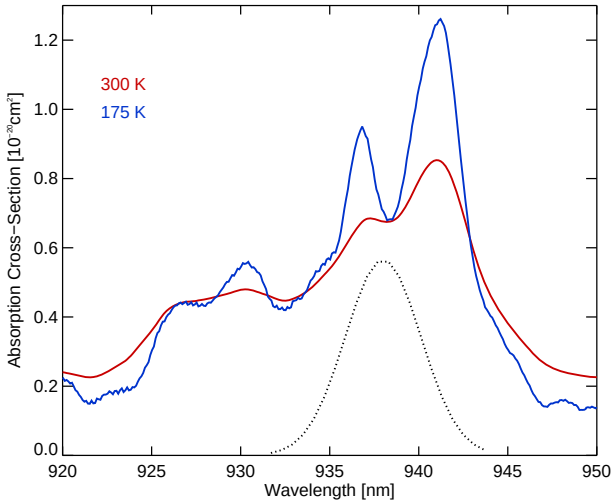

Fig. 6. Absorption spectra for Yb:YAG at 175 K (blue) and 300 K (red). Shown for comparison is a Gaussian-shaped spectrum with 5 nm FWHM (dotted line). From [23].

The effect of varying the width of the (Gaussian) pump spectrum is shown in Fig. 7. Because of the finite width of the absorption lines, the maximum obtainable efficiency drops with increasing width of the pump spectrum. The effect is already noticeable for $\Delta\lambda_P > 1$ nm in both cases, which is much less than the FWHM-width of the absorption line. Because of the asymmetry of the absorption spectrum, the optimum centre wavelength also shifts to smaller values with increasing $\Delta\lambda_P$. For $\Delta\lambda_P > 2$ nm the dependence of η_P on $\Delta\lambda_P$ is approximately linear in both cases. A linear fit yields a slope of $-0.58\%/\text{nm}$ in the room temperature case and $-0.47\%/\text{nm}$ in the low temperature case. In relative terms ($\Delta\eta_P/\eta_P$), this translates to $-1.6\%/\text{nm}$ and $-0.94\%/\text{nm}$ for room and low temperature scenarios, respectively. Hence the sensitivity to $\Delta\lambda_P$ is significantly lower in the low temperature case.

Whereas every data point in Fig. 7 was calculated with optimum $\lambda_{c,P}$ and optimum N_{col}, it is also interesting to explore the sensitivity of a fixed amplifier configuration, optimised for a certain set of parameters, to changes in the pump spectrum. Figure 8(a) shows how η_P changes for an amplifier with a fixed N_{col} (optimised for the scenarios listed in Table 1) if $\lambda_{c,P}$ is de-tuned from the optimum value. The sensitivity is clearly greater for the room temperature scenario, where η_P drops by 2% if $\lambda_{c,P}$ is de-tuned by $+1.4$ nm or by -1.7 nm. For the low temperature scenario, the respective values are $+1.7$ nm and -2.3 nm. Figure 8(b) shows the dependence of η_P on $\Delta\lambda_P$ for otherwise fixed parameters. Again, the sensitivity to changes is greater in the room temperature case.

In conclusion, we can state that an amplifier operated at lower temperature places less demand on the pump source, despite the narrower features in the absorption spectrum. This holds

#157898 - $15.00 USD Received 11 Nov 2011; revised 5 Dec 2011; accepted 5 Dec 2011; published 14 Dec 2011

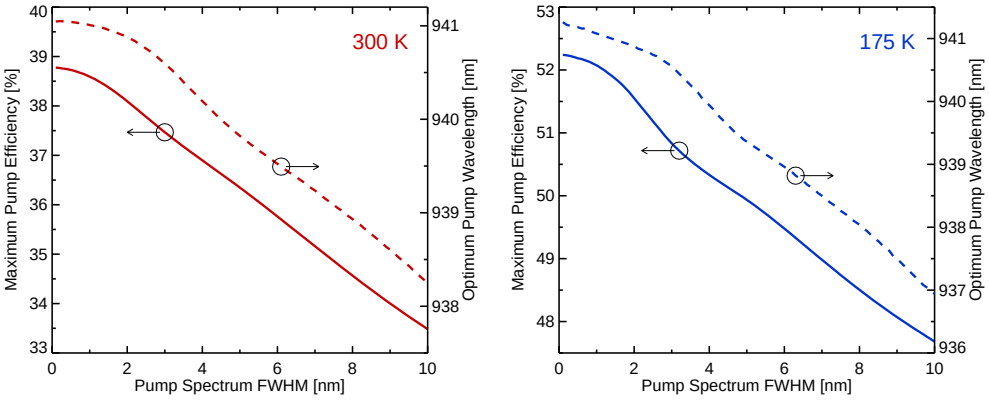

Fig. 7. Maximum pump efficiency (solid line) as function of pump spectral width for room temperature scenario (left) and low temperature scenario (right). Also shown is the optimum centre wavelength (dashed line) as function of pump spectral width.

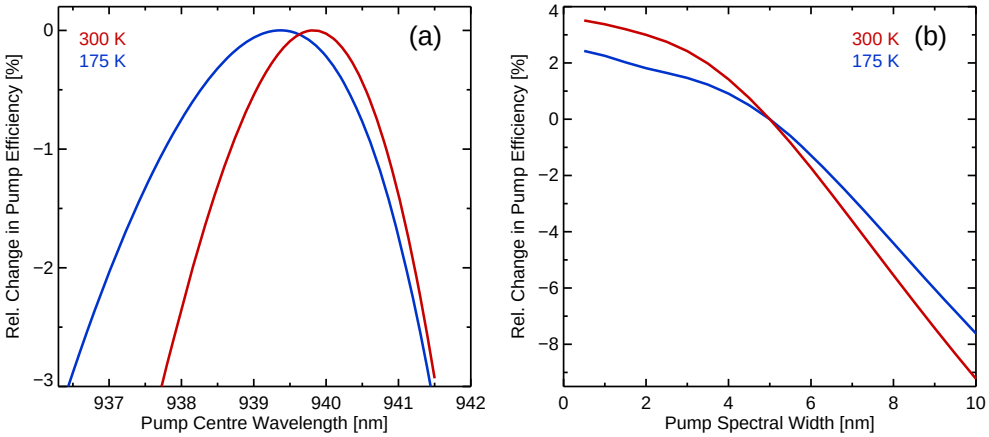

Fig. 8. Change in pump efficiency as function of pump centre wavelength (a) and of pump spectral width (b), for room temperature scenario (red) and low temperature scenario (blue). All other parameters were fixed and optimised for the scenarios listed in Table 1.

true both for the design phase, where other parameters can still be optimised to adapt to a given spectral width of the pump source, and for the operation phase, where a low temperature amplifier is less sensitive to changes in the pump spectrum, caused, for example, by drifts in pump diode operating temperature or current, or by ageing of the pump diodes.

3.6. Effect of advanced pump schemes

We have shown in Section 3.3 that reabsorption severely limits the pump efficiency at room temperature and that reabsorption losses grow with N_{col}. To overcome this problem, N_{col} needs to be reduced while maintaining a high level of pump absorption. One way of achieving this is multi-pass pumping which is already used extensively in thin disk lasers [29], and has recently also been shown to be effective in transmission-type amplifiers [20]. For a quantitative assessment we have modelled the dependence of η_P on N_{col} for our room temperature scenario assuming 1, 2, and 4-pass pumping. The results of the calculations are shown in Fig. 9(a).

As expected, multi-pass pumping increases η_P for any given N_{col} as pump absorption is

#157898 - $15.00 USD Received 11 Nov 2011; revised 5 Dec 2011; accepted 5 Dec 2011; published 14 Dec 2011

increased. The main increase of η_P is, however, caused by the fact that the maximum η_P is achieved at lower N_{col}, leading to greatly reduced reabsorption losses. This is due to an increased β as is shown in Fig. 9(b). Here, a constant doping level of 1% is assumed for all three scenarios, meaning that the gain medium has to become shorter for a higher number of pump passes. It can also be seen that β not only grows on average with increasing number of pump passes, but it also becomes more uniform, which is beneficial for ASE management [31]. Despite the reduced N_{col} at the maximum of η_P, the pump absorption still increases with the number of pump passes. The fraction of absorbed pump light is 89.2%, 94.6%, and 97.5% for the 1, 2, and 4-pass scenarios, respectively.

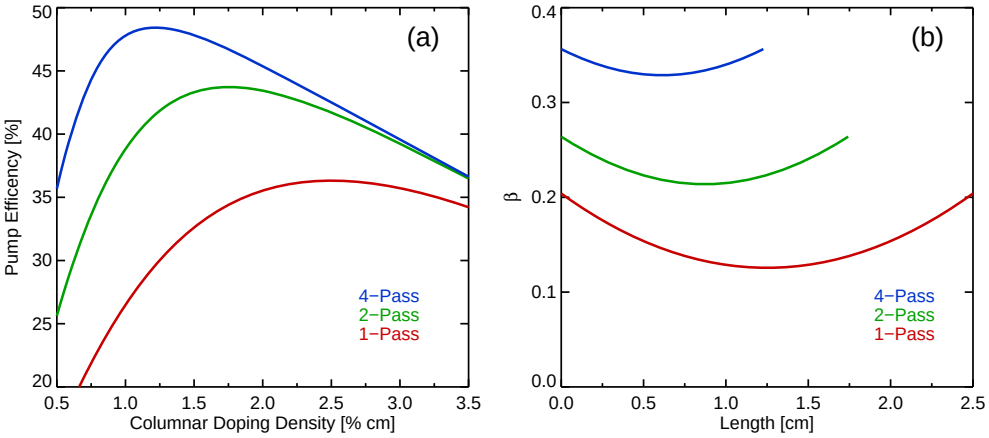

Fig. 9. Panel (a): Pump efficiency for room temperature scenario as function of columnar doping density for 1, 2, and 4-pass pumping. Panel (b): Distribution of upper state population β along optical axis for room temperature scenario with 1, 2, and 4 pump passes.

4. Concept for a large-aperture, cryogenically-cooled laser amplifier

In the following sections we will present a concept for a large aperture diode pumped Yb:YAG amplifier which is suitable for producing high-energy ns-pulses, which offers a multitude of benefits compared to other concepts.

4.1. Description of concept

Figure 10 illustrates the conceptual design of our amplifier architecture, inspired by the Mercury laser [15]. It consists of a series of square ceramic Yb:YAG slabs (for use with square pump and extraction beams) with a co-sintered Cr^{4+}:YAG cladding. The slabs are held in aerodynamically shaped vanes with a small gap between adjacent vanes. A flow of cold helium gas is forced through those gaps to provide cooling. This multi-slab architecture also provides the possibility to employ slabs with differing doping concentrations.

4.2. Main aspects and benefits of concept

4.2.1. Ceramic Yb:YAG gain medium

The benefits of Yb^{3+} as the active laser ion have already been briefly outlined in Section 1, namely the long fluorescence lifetime, which maximises the stored energy for a given pump intensity (see Eq. (2)); the low quantum defect that leads to high optical-to-optical efficiency; the simple level scheme which eliminates parasitic processes like excited stated absorption and

#157898 - $15.00 USD Received 11 Nov 2011; revised 5 Dec 2011; accepted 5 Dec 2011; published 14 Dec 2011

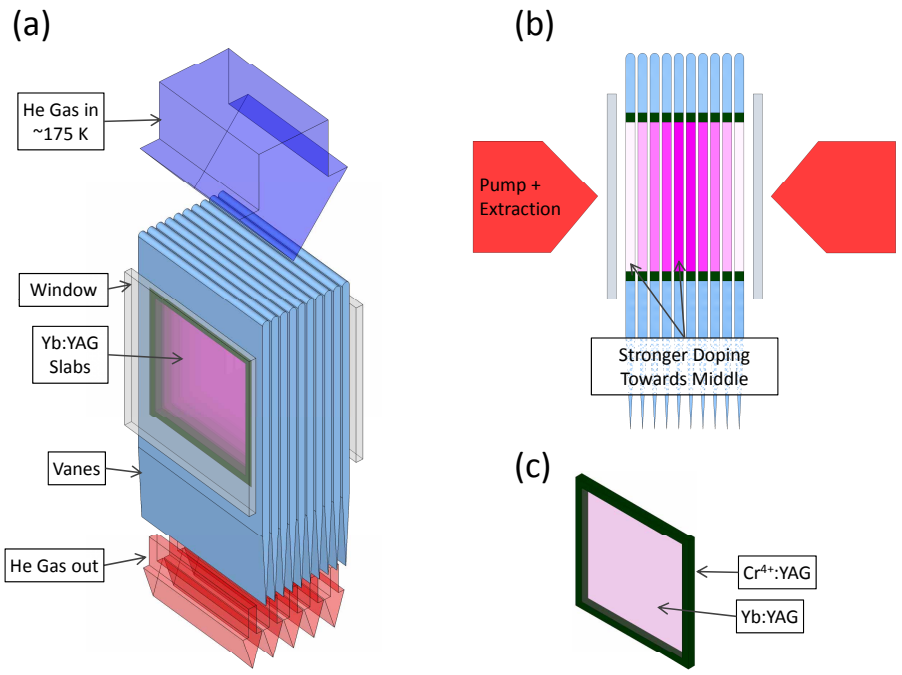

Fig. 10. Isometric view (a) and side view (b) of the cryogenic gas cooled multi-slab amplifier concept. An individual amplifier slab is shown in (c).

concentration quenching; and the absorption spectrum, which is relatively broad and coincides with the wavelength region where diode lasers offer the highest power, efficiency, and reliability. When YAG is used as the host material, Yb^{3+} also offers a reasonably high σ_e, enabling efficient energy extraction at moderate fluence levels.

In addition, the choice of ceramic YAG as the host material offers good thermo-mechanical properties such as thermal conductivity and thermal shock parameter which are required to cope with high average powers. The material can be manufactured in large sizes which is required to cope with high pulse energies, and finally it enables the production of compound structures such as Yb:YAG/Cr^{4+}:YAG. As Cr^{4+}:YAG is strongly absorbing at the emission wavelength of Yb:YAG, it can be used as an index-matched absorber medium for effective suppression of parasitic oscillations [32].

4.2.2. Distributed face cooling

This cooling approach minimises thermo-optical distortions of the transmitted beam, as the heat flow and hence the thermal gradients in the active medium are mainly parallel to the beam. Furthermore, it enables a low overall aspect ratio (gain medium diameter divided by total thickness) while offering a high surface-to-volume ratio. The former aspect is important for minimising ASE losses because a high single pass gain can be achieved while keeping the gain coefficient and hence the maximum transverse gain-length product low. The high surface-to-volume ratio is required for effective heat removal at high average power operation. Helium gas is used as the cooling medium as it offers high thermal conductivity and the scattering losses caused by refractive index fluctuations are much lower compared to other candidate gases [33]. Furthermore, He gas is compatible with cryogenic operation down to temperatures below 10 K.

#157898 - $15.00 USD Received 11 Nov 2011; revised 5 Dec 2011; accepted 5 Dec 2011; published 14 Dec 2011

4.2.3. Cryogenic operation

The positive effect of cryogenic operation on pump efficiency has been discussed extensively in Section 3. Furthermore, the thermo-mechanical and thermo-optical parameters of YAG improve with decreasing temperature [34, 35], which results in a reduction of adverse effects like thermally-induced wave front distortion and thermally-induced birefringence. Another benefit of low temperature operation, which greatly affects extraction efficiency and therefore overall system efficiency, is the fact that the emission cross section of Yb:YAG increases with decreasing temperature [36, 37]. Figure 11 shows a similar graph as Fig. 5, but this time also showing $\exp(G_o)$, the small-signal gain, as a function of pump intensity for our two scenarios and a modified room temperature scenario with 2-pass pumping. For the low temperature scenario, $\exp(G_o)$ increases much faster with I_P. For the I_P values specified for our scenarios, $\exp(G_o) = 3.9$ for the low temperature scenario, but for the room temperature scenario, $\exp(G_o)$ only equals 2.0, despite the two times higher I_P. Multi-pass pumping can improve pump efficiencies at room temperature, the inaccessible excited fraction β_{min}, however, is not affected by the pumping scheme and is significantly larger at room temperature. The problem of very low gain values at room temperature also remains. Multi-pass pumping would also add significant complexity to the optical set-up and would require very bright pump sources to be feasible at all in large-aperture systems. The σ_e values assumed for the calculations were $1.8 \times 10^{-20}\,\mathrm{cm}^2$ and $5.2 \times 10^{-20}\,\mathrm{cm}^2$ for the room and low temperature scenarios, respectively [36].

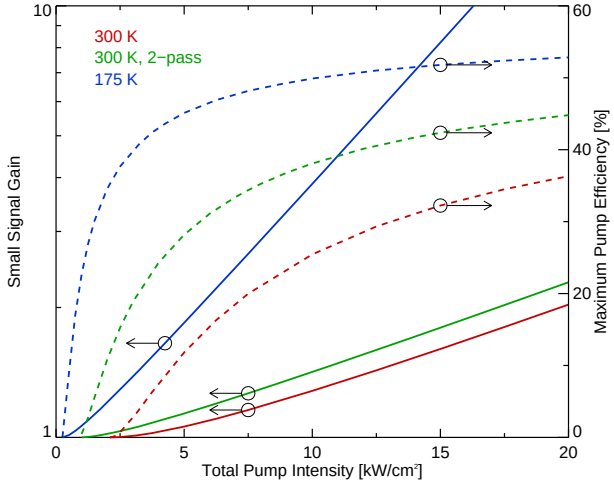

Fig. 11. Small-signal gain (solid lines) and maximum pump efficiency (dashed lines) as function of pump intensity for room temperature scenario (red), room temperature scenario with 2-pass pumping (green), and low temperature scenario (blue).

4.2.4. Variable doping

The multi-slab architecture offers the possibility to employ slabs with different doping levels within the amplifier. This way, the doping profile can be tailored such that the same amount of pump energy is absorbed in each slab, which yields benefits in terms of thermal management and reduces the overall thickness of the amplifier, as will be shown in Section 4.3.2.

4.3. Model calculations

We have used our numerical model described in Section 2.2 in order to establish initial design parameters for an amplifier sized for 1 kJ output energy. A laser based on this amplifier could

#157898 - $15.00 USD Received 11 Nov 2011; revised 5 Dec 2011; accepted 5 Dec 2011; published 14 Dec 2011

form a building block for an inertial fusion reactor or it could pump a multi-PW fs-laser used for particle acceleration or other types of secondary sources.

4.3.1. Size-independent parameters

We have based our design on the low-temperature scenario as laid out in Table 1 as it provides a good balance between laser-physical performance such as gain and efficiency and technical requirements such as spectrum and brightness of diodes, damage threshold of optics, and power consumption of the cryogenic cooling plant. The parameters put into the model and obtained from the model are summarised in Table 2.

Table 2. Size-independent parameters for high energy amplifier design.

Parameter	Value
Pump intensity (total)	$10\,\mathrm{kW\,cm^{-2}}$
Pump duration	1 ms
Pump spectral width (FWHM)	5 nm
Pump central wavelength	939.4 nm
Columnar doping density	3.3 % cm
Pump efficiency	49.9 %
Small-signal gain	3.9

4.3.2. Size-dependent parameters

The aperture of the amplifier is determined by the total energy to be extracted. The energy accessible for extraction in our scenario is $5\,\mathrm{J\,cm^{-2}}$. If 100 % of that energy could be extracted without losses, the aperture would need to be $200\,\mathrm{cm^2}$, or $14\,\mathrm{cm} \times 14\,\mathrm{cm}$. In practice, it is probably more realistic to assume an extraction efficiency of only 50 %. Rather than doubling the aperture of the amplifier, we suggest using two amplifier heads in series, similar to the Mercury laser [15]. As long as the resulting increased extraction fluence is still tolerable, the laser is then more compact and shows a higher single-pass gain, reducing the number of extraction passes required for a given input energy.

The number of slabs required is governed by thermal management considerations. The slabs should have a high aspect ratio in order to minimise radial heat flow which results in thermo-optically induced aberrations. The absolute thickness of the slabs should be low enough to keep the temperature difference between slab centre and slab surface at acceptable levels. Finally, the number of the slabs should be high enough to ensure sufficient heat removal for an acceptable coolant mass flow in a single cooling channel. Initial thermal modelling suggests that choosing 10 slabs satisfies these requirements.

Thickness and doping concentration of the amplifier slabs are governed by ASE management considerations. We have used the rule that the gain-length product $G_{ASE} = \int_0^D g_o \mathrm{d}l$ must not exceed 3 for any straight path of length D inside the amplifier [25]. In our case the maximum G_{ASE} is found along the diagonal across the surface of the amplifier slabs where g_o is constant and $D = 20\,\mathrm{cm}$ and hence g_o must not exceed $0.15\,\mathrm{cm^{-1}}$.

If all slabs had the same doping concentration, each slab would need to be 19 mm thick with a doping concentration of 0.18 %. In the constant-doping case the distribution of g_o and absorbed energy is very non-uniform, falling off steeply from the outside towards the centre.

If on the other hand the doping of each slab is adjusted such that $g_{o,max}$ is reached in every slab, the distribution of g_o and hence absorbed energy become much more uniform and the thickness of the slabs can be significantly reduced. Figure 12 shows the distribution of g_o and

#157898 - $15.00 USD Received 11 Nov 2011; revised 5 Dec 2011; accepted 5 Dec 2011; published 14 Dec 2011

doping concentration in an optimised 10-slab configuration, with the thickness of each slab now being only 10.3 mm, a reduction by 46% compared to the constant doping case.

A possible layout and predicted laser performance parameters of a 1 kJ beam line, such as extraction efficiency, pulse shape, and B-integral, together with thermal modelling results have been published in [38, 39].

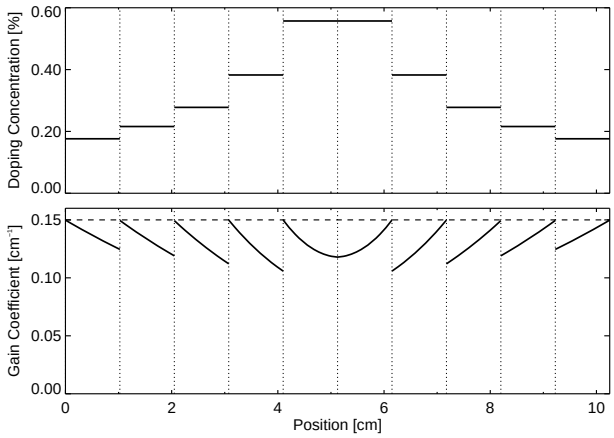

Fig. 12. Doping concentration (upper panel) and gain coefficient (lower panel) for 10-slab amplifier with variable doping. Vertical dotted lines denote slab boundaries, horizontal dashed line denotes maximum allowed gain coefficient.

5. Conclusion

We have presented a comprehensive numerical model for a pulsed, end-pumped DPSSL Yb:YAG amplifier. We have shown that, compared to room temperature operation, low temperature operation yields much higher efficiency and gain at realistic pump and extraction fluence levels. The demands on the pump source in terms of spectral width and wavelength stability are also relaxed in the low temperature regime. The material and spectroscopic properties of Yb:YAG which are very favourable for high repetition rate, high energy laser amplifiers are further improved at low temperatures.

Based on the results of our modelling, we have presented a conceptual design of a cryogenic, gas-cooled, multi-slab amplifier that can achieve high levels of gain and energy storage while offering a large surface area for effective cooling and a low transverse gain-length product for minimising ASE losses. This concept is scalable to any size from the few-J to the multi-kJ level, because the overall thickness of the gain medium can be chosen freely without compromising cooling, and because, unlike single crystals, the ceramic gain medium can be manufactured in arbitrarily large sizes.

A prototype laser, called DiPOLE, based on the proposed amplifier architecture is currently being tested in order to validate the concept. First experimental results will be published shortly.

Acknowledgments

We would like to thank Daniel Albach, Jean-Christophe Chanteloup and Joachim Hein for inspiring discussions. We thank David C. Brown for providing Yb:YAG absorption cross section data in tabulated form.

#157898 - $15.00 USD Received 11 Nov 2011; revised 5 Dec 2011; accepted 5 Dec 2011; published 14 Dec 2011